Title: *In situ* high spatial resolution $^{87}Sr/^{86}Sr$ ratio determination of two Middle Pleistocene (c.a. 580 ka) *Stephanorhinus hundsheimensis* teeth by LA–MC–ICP–MS

Author: Federico Lugli Anna Cipriani Carlo Peretto Maurizio Mazzucchelli Daniele Brunelli

PII: S1387-3806(16)30340-2
DOI: http://dx.doi.org/doi:10.1016/j.ijms.2016.12.012
Reference: MASPEC 15735

To appear in: *International Journal of Mass Spectrometry*

Received date: 6-9-2016
Revised date: 1-12-2016
Accepted date: 13-12-2016

Please cite this article as: Federico Lugli, Anna Cipriani, Carlo Peretto, Maurizio Mazzucchelli, Daniele Brunelli, In situ high spatial resolution 87Sr/86Sr ratio determination of two Middle Pleistocene (c.a.580 ka) Stephanorhinus hundsheimensis teeth by LA–MC–ICP–MS, International Journal of Mass Spectrometry http://dx.doi.org/10.1016/j.ijms.2016.12.012

In situ high spatial resolution $^{87}Sr/^{86}Sr$ ratio determination of two Middle Pleistocene (c.a. 580 ka) *Stephanorhinus hundsheimensis* teeth by LA–MC–ICP–MS

Federico Lugli[a,*], Anna Cipriani[a,b], Carlo Peretto[c], Maurizio Mazzucchelli[a], Daniele Brunelli[a]

[a] Department of Chemical and Geological Sciences, University of Modena and Reggio Emilia, Via Campi, 103 – 41125 Modena, Italy.

[b] Lamont-Doherty Earth Observatory, Columbia University, Palisades, New York 10964, USA.

[c] Dipartimento Studi Umanistici, Sezione di Scienze Preistoriche e Antropologiche, Università degli Studi di Ferrara, LT, TekneHub, Ferrara, Italy.

* Corresponding author – e-mail: federico.lugli@unimore.it

Graphical abstract

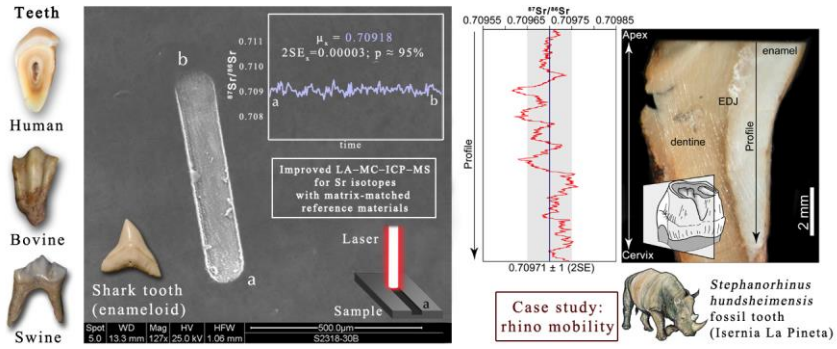

Highlights

- $^{87}Sr/^{86}Sr$ determination by LA–MC–ICP–MS of biogenic apatites strengthened.
- Using of three matrix-matched in-house reference materials.
- Two Middle-Pleistocene rhino fossil teeth analysed in high-spatial resolution.

Abstract

Bone and tooth tissues are important biological archives to study eating habits and provenance of ancient humans and animals. By taking advantage of the high spatial resolution offered by the Laser Ablation Multi Collector Inductively Coupled Plasma Mass Spectrometry (LA–MC–ICPMS) technique, we investigated the $^{87}Sr/^{86}Sr$ intra-tooth variability of two *Stephanorhinus hundsheimensis* tooth fragments from the Middle Pleistocene site of Isernia La Pineta. We detected significant Sr isotopes variability within the rhinos tooth enamel (enamel average ±2σ: sample RH–IS30 0.70951 ± 0.00014; sample RH–IS26 0.70976 ± 0.00015) with values higher than the "local" $^{87}Sr/^{86}Sr$ ratio (dentine average ±2σ: sample RH–IS30 0.70918 ± 0.00013; sample RH–IS26 0.70934 ± 0.00009). This is likely linked to a different water and food intake with a Sr isotopic signature similar to volcanic soils nearby (Roccamonfina: from 0.7093 to 0.7100; Colli Albani: > 0.7100) and supports the idea that the *Stephanorhinus hundsheimensis* species moved around seasonally. The improvement of non-destructive, accurate and precise analytical methods to decrypt the information hidden within bone and tooth hard tissues of archeological material is crucial to- unravel critical questions about evolution, migration and ecology of human and animals. We have successfully took upon this challenge using three matrix-matched standards, with variable Sr concentration (c.a. 100 to 1000 ppm), to correct unresolved interferences arising from LA analyses.

Keywords: LA–MC–ICP–MS; strontium isotopes; bioapatite; enamel; rhino

1. Introduction

Strontium isotopes have become an important tool in palaeontological research to track ancient human and animal migratory patterns and provenance (e.g. Price et al., 2002; Bentley, 2006; Evans et al., 2006; Montgomery et al., 2007; Copeland et al., 2011; Bentley et al., 2012). Tooth enamel, if available, is the best material for geochemical investigations because it is made of a ~ 96% mineralized hydroxyapatite more resistant to diagenesis (Bentley, 2006) and is an elemental and Sr isotope archive of the individual life.

Strontium substitutes calcium in the hydroxyapatite of bones and teeth (Burton et al., 1999) and its $^{87}Sr/^{86}Sr$ ratio is directly related to the ratio of plants and water ingested by humans and animals (e.g. Pate, 1994; Burton and Wright, 1995; Bentley, 2006).

Strontium ions enter the ecosystem through the weathering of the local bedrock, which usually retains a peculiar $^{87}Sr/^{86}Sr$ ratio related to the petrogenetic process, the age and the initial rubidium content of the rock itself. Thus, analysing the $^{87}Sr/^{86}Sr$ ratio of dental and bone tissues can help identify the place where the tissue has formed or remodelled. Given that enamel forms during the individual growth and preserves incremental features of its formation, small scale isotopic investigations allow to detect temporal variations in the Sr isotopic composition of the animal life even within one tooth (e.g. Balasse, 2003; Tafforeau et al., 2007; Martin et al., 2008; Britton et al., 2011). In such sense, the growth lines or bands visible by microscopic observations of teeth, the so-called Retzius lines (or striae of Retzius), are the best-known long-term period incremental features of the dental enamel and represent the successive apposition of forming enamel (Smith and Tafforeau, 2008). The time between the formation of two striae of Retzius is between 2 and 12 days in primate teeth and about 7 days in rhino teeth (e.g. Tafforeau et al., 2007; Smith and

Tafforeau, 2008). This time-span, namely periodicity, can be estimated counting the visible laminations (i.e. daily isochrones of the enamel deposition) per Retzius band (Tafforeau et al., 2007).

Traditionally, Sr isotopes have been analyzed by Thermal Ionization Mass Spectrometry (TIMS) and MC–ICPMS requiring total dissolution of a portion of the sample and chemical separation of strontium (e.g. Li et al., 2013). The recent development of the Laser Ablation system (LA) coupled with a Multi Collector Inductively Coupled Plasma Mass Spectrometer (MC–ICPMS) has allowed high spatial resolution analyses with a micro-destructive approach, with the opportunity to analyze even small tooth fragments and unravel possible isotopic heterogeneity at the small scale within the tooth itself (Horstwood and Nowell, 2005; Copeland et al., 2008; Horstwood et al., 2008; Richards et al., 2008; Simonetti et al., 2008; Copeland et al., 2010; Copeland et al., 2011; Balter et al., 2012). This technique can be particularly helpful when dealing with small ancient enamel fragments of migratory animals or precious remains that cannot be destroyed by canonical dissolution methods.

Despite the clear advantage of this technique, LA–MC–ICPMS analyses have some issues mainly related to analytical artefacts. In particular, during analysis several isobaric interferences are known to form; whilst some are routinely and properly corrected by many laboratories (e.g. Rb and Kr), others may hinder the achievement of precise and accurate results (e.g. REE^{2+}, $^{40}Ca^{46}Ca$, $^{46}Ca^{40}Ar$, $^{40}Ca^{31}P^{16}O$ and $^{40}Ar^{31}P^{16}O$; Copeland et al., 2008; Horstwood et al., 2008; Vroon et al., 2008; Willmes et al., 2016).

In this work, we investigated the $^{87}Sr/^{86}Sr$ ratio intra-tooth variability of two *Stephanorhinus hundsheimensis* teeth (LA samples *n* = 82) from the Middle

Pleistocene site of Isernia La Pineta (Molise, Italy), to unravel possible variations within the tooth enamel and to try to reconstruct a migratory pattern for the *Stephanorhinus hundsheimensis* species in the area. Beside the *Bison schoetensacki,* this is the second most represented taxa in the area (Ballatore and Breda, 2013; Peretto et al., 2015). We analyzed our two samples in order to detect if incremental fluctuations of the $^{87}Sr/^{86}Sr$ ratio, i.e. representing temporal variations in the Sr isotopic composition, were preserved in the enamel and if they correlated with the structural growth features of the tooth.

2. Materials and Methods

Two fragments (a longitudinal and a transversal section) of *Stephanorhinus hundsheimensis* molars (RH–IS30 and RH–IS26) were collected among the non-musealized samples found at the Isernia La Pineta site. Sample RH–IS30 was collected from the archaeological layer called 3s10 and sample RH–IS26 from the 3c layer (for more details about the stratigraphy see Peretto et al., 2015). Argon–argon dating ($^{40}Ar/^{39}Ar$) suggests an age of about 580 ka for both layers (Peretto et al., 2015). The surface of both samples was analyzed in detail, with 80 LA short linear scans composing four profiles (Fig. 1 and Fig. 2; Profiles A, B, C and D). We noticed that short linear scans gave better results than spots in terms of signal stability. Of these short scans, 60 were performed on the enamel surface and 20 on the dentine surface.

Dentine is usually not a good indicator of provenance because of its high susceptibility to diagenetic contamination (e.g. Bentley et al., 2006) whereas enamel is generally less affected by diagenesis and represents the best target. In the case of

samples that due to their uniqueness cannot be cut to expose their inner parts, scientists have to rely on analyses of the outer enamel (e.g. Copeland et al., 2011).

Sample RH–IS26 was also tested with a slightly different method using continuous long scan profiles for the entire length of the enamel portion. We obtained two profiles: one (profile E) on the inner and one (profile F) on the outer surface of the enamel as shown in Fig. 3.

Following Horstwood et al. (2008), we have also selected and analyzed four bioapatites with different Sr concentration to establish our matrix-matched standard materials given the unavailability of solid bioapatite standards on the market. We selected a shark tooth with a Sr concentration of ~1100 ppm (average 1101 ± 47 ppm), a bovine tooth with a Sr concentration of ~350 ppm (average 347 ± 18 ppm), a swine tooth with a Sr concentration of ~250 ppm (average 253 ± 31 ppm) and a human tooth with a Sr concentration of ~100 ppm (average 104 ± 25 ppm). The shark tooth (*Carcharhinus leucas*, Müller and Henle, 1839) was purchased from an online specialized shop. Shark tooth enameloid is composed largely of fluorapatite ($Ca_5(PO_4)F$) and minor hydroxyapatite ($Ca_5(PO_4)OH$) (Vennemann et al., 2001), however, their Ca/P molar ratio and the relative content of Ca^{2+} and PO_4^{3-} are similar to mammal enamel (Enax et al., 2012). The swine tooth (SUS–Sr1) and the bovine tooth (BOS–Sr1) were collected from a roman archaeological site in Ravenna (Italy), while the human tooth (ROCht421) was selected among the best-preserved mummies teeth buried in the archaeological site of Roccapelago (16^{th} and the 18^{th} century AD, Modena, Italy; Lugli et al., *accepted*). Prior to LA-analyses, portions of our in-house bio-standards were analysed in solution by MC–ICP–MS to obtain the reference $^{87}Sr/^{86}Sr$ value.

2.1. Thin section preparation

Incremental growth features of the transversal section of tooth RH–IS26 were studied under a transmitted-light petrographic microscope (Fig. 5). A petrographic thin section of the sample was prepared by embedding the tooth in polyester resin, gluing onto a microscope glass section, cutting in a ~1 mm section with a diamond saw and manually polishing to a thickness of 100 µm with decreasing-size polishing paper and aluminium oxide (Tafforeau et al., 2007). Observation and counting of Retzius lines was performed in polarized transmitted light with an Olympus BH-2 petrographic microscope.

2.2. Dissolution method MC–ICPMS

Samples were prepared at the Department of Chemical and Geological Sciences of the University of Modena and Reggio Emilia. The tooth enamel was manually separated from the dentine using a dentist drill. After a macroscopic cleaning with small brushes, each enamel chunk was boiled in MilliQ® for 1h to remove any possible superficial residue of organic matter, rinsed repeatedly with MilliQ® and then sonicated in an ultrasonic bath for 30 minutes. Before dry down, samples were rinsed 3 times with MilliQ® and once with high purity acetone. Samples were digested in 1ml of suprapure 14N HNO_3, evaporated to dryness and dissolved in 3ml of 3N HNO_3. After centrifuging, samples were loaded into 300 µl volume columns filled with Eichrom Sr spec–resin and washed with 3N HNO3. Sr was finally eluted with several reservoirs of MilliQ® water (Deniel and Pin, 2001).

The $^{87}Sr/^{86}Sr$ isotopic composition of the samples was determined using a double focusing MC–ICPMS with a forward Nier–Johnson geometry (Thermo Fisher

Scientific, Neptune™) housed at the Centro Interdipartimentale Grandi Strumenti (CIGS) of the University of Modena and Reggio Emilia.

Seven of the nine Faraday detectors, fitted with $10^{11}\Omega$ resistors, were used to collect signals of the following masses: ^{82}Kr, ^{83}Kr, ^{84}Sr, ^{85}Rb, ^{86}Sr, ^{87}Sr, ^{88}Sr. Solutions were diluted to 200 ppb of Sr and introduced into the Neptune via quartz spray chamber and a 100 microliter/min nebulizer. The ^{88}Sr signal of the shark tooth (~1100 ppm), after proper dilution to 200 ppb, was ~15 V and the blank level (0.5 HNO_3) 0.02 V. Samples and standards were analyzed in a static multi–collection mode in a single block of 100 cycles, with an integration time of 8 s per cycle. A classic bracketing sequence [blank/standard/blank/sample/blank] has been used to monitor any eventual drift of the instrument.

Masses 82 and 83 were collected to monitor the presence of Kr in the argon. Data were corrected using a $^{86}Kr/^{83}Kr$ ratio of 1.505657. Mass 85 was used to correct the signal on mass 87 for the presence of isobaric Rb, using a $^{87}Rb/^{85}Rb$ ratio of 0.3856656. Mass bias normalization, through exponential law, was carried out using a $^{88}Sr/^{86}Sr$ ratio of 8.375209. Mass fractionation for both Kr and Rb has been assumed equal to that one of Sr. The $^{87}Sr/^{86}Sr$ ratios were corrected for instrumental bias to an NBS–987 value of 0.710260 ± 0.00002 (Ehrlich et al., 2004; Durante et al., 2015). Repeated analyses of the NBS–987 yielded a $^{87}Sr/^{86}Sr$ ratio of 0.710272 ± 0.000013 (2σ; n = 8, corresponding to an external reproducibility of 18 ppm). The long–term reproducibility (*c.a.* three years of analyses; n > 2000) of the instrument yielded a $^{87}Sr/^{86}Sr$ ratio of 0.71027 ± 0.00002 (2σ; Durante et al. 2015).

2.3. Laser ablation method MC–ICPMS

The teeth portions chosen for laser analysis were cleaned with brushes, washed with

MilliQ® water and carefully dried down before introduction into the LA sample holder.

Sr data were acquired with the Neptune MC–ICPMS, coupled to a 213 nm Nd:YAG laser ablation system (New Wave Research™) housed at CIGS–UNIMORE (Table 1). Before LA analyses, the instrument was tuned using the NBS–987 standard solution, monitoring both the signals and the significant isotopic ratios.

All nine Faraday detectors were used to acquire peaks of the following masses ^{82}Kr, ^{83}Kr, ^{84}Sr, ^{85}Rb, ^{86}Sr, ^{87}Sr, ^{88}Sr and half masses 85.5 and 86.5. Half masses 86.5 and 85.5 were monitored to check for the contribution of doubly charged Rare Earth Elements ($^{171}Yb^{2+}$ and $^{173}Yb^{2+}$). Usually these signals are below the detection limit of the instrument (LOD), therefore the correspondent detectors were equipped with 10^{12} Ω resistors.

We used the “on peak zero” method to correct for Kr interferences (Davidson et al., 2001; Vroon et al., 2008) by measuring a 60 s gas background for each mass before each analysis and subtracting the signal of each detector to the measured value of the sample. After background subtraction, the remaining signal of mass 82, was used to check the formation of Ca dimers and argides, isobars to masses ^{84}Sr, ^{86}Sr, ^{87}Sr and ^{88}Sr (Woodhead et al., 2005). Typically, Ca dimer and argide signals on mass 82 are around 0.1 mV. Likewise, the remaining signal of mass 83 (after Ca dimers argides subtraction) was used to correct for the presence of $^{166}Er^{2+}$ (Copeland et al., 2010). Rb interferences were corrected using the same procedure followed for the dissolution method. We note here that the ^{85}Rb signal during our analytical sessions has always been lower than 1 mV.

We employed a linear ablation pattern (100 x 500 µm) to sample the tooth enamel surfaces in order to limit laser-induced elemental fractionations and to improve the beam size stability (Vroon et al., 2008; Guillong and Günther, 2002).

Our daily LA–MC–ICPMS tuning is based on a 3-step protocol using our ST1 in house-reference material. During the first step, ST1 is analysed to optimize the machine parameters tuning for the maximum signal intensity on ^{88}Sr. Second, background signal intensities on ^{83}Kr and ^{82}Kr are monitored. Ideally they have to be as low as possible and, as also observed by Jackson and Hart (2006), the $^{83}Kr/^{82}Kr$ ratio has to be maintained near ~1 to obtain the best results in term of precision and accuracy. Finally, the $^{87}Sr/^{86}Sr$ ratio of the ST1 standard is measured and machine parameters are tuned until the desired ratio (~0.7092) is obtained. Laser data were acquired with a block of 200 cycles, an integration time of 0.5 s and a laser spot size of 100 µm. The surface of the tooth was pre–ablated before each analysis. Summary of the typical LA parameters used during our sessions are presented in Table 1.

The two continuous long LA scan profiles obtained for tooth RH–IS26 were acquired with a block of 2000 cycles and an integration time of 0.5 s. We used a laser spot size of 100 µm and a line length of about 6 mm. We calculated a moving average of the cycles with a period of 100.

As reported by several authors, during LA analyses is difficult to address the specific interferences that contribute to the fractionation of the $^{87}Sr/^{86}Sr$ ratio (e.g. Whoodhead et al., 2005; Balter et al., 2008; Horstwood et al., 2008; Simonetti et al., 2008; Vroon et al., 2008; Nowell and Horstwood, 2009; Lewis et al., 2014). The proposed $^{40}Ca^{31}P^{16}O$ interference on mass 87 is still a matter of debate. In fact, while several authors claim its existence (e.g. Horstwood et al., 2008; Simonetti et al., 2008; Lewis et al., 2014), others never experienced it (e.g. Copeland et al., 2008; Müller and Anczkiewicz, 2016). More recently, Willmes et al. (2016) have attributed the interference on mass 87 to the $^{40}Ar^{31}P^{16}O$ molecule, because of the omnipresence of Ar in the plasma atmosphere. They correct this polyatomic

interference adding a flux of nitrogen gas to reduce the formation of oxides within the plasma and monitoring mass 71 ($^{40}Ar^{31}P$) as a proxy of the $^{40}Ar^{31}P^{16}O$ oxide production. This method seems to solve the interference problem related to mass 87 but largely reduces (factor of 2–3) the intensity of Sr signals, a serious problem when dealing with low-Sr samples. They partially resolve this issue by employing a larger spot size (~250 µm), resulting in a more intense signal because of the increased volume of ablated material (Vroon et al., 2008), but with the obvious consequence of a more destructive analysis. They also suggest that a valid approach to correct for the bias arising from mass 87-interferences is a calibration correction with a series of known standards (Willmes et al., 2016; Horstwood et al., 2008).

In addition to mass-87 interference, LA isotope analyses often endure the so-called laser-induced elemental/isotope fractionation, as observed for other isotopic systematics (i.e. U–Pb), which may bias the final isotope ratio (see Horn 2008; Vroon et al., 2008). Moreover, many unknown interferences may form in the MC–ICP–MS atmosphere, mainly because of the bonds of oxygen and argon with elements of the sample matrix ionised within the plasma (Vroon et al., 2008). No matter how or why interferences arise during Sr LA analysis of a particular material, the concurrent analysis of a set of matrix-matched standards is a proper approach to monitor and correct the Sr fractionation issues, as demonstrated by Horstwood et al. (2008) and reiterated by Willmes et al. (2016). Standards with matrix equal to the samples are ideal because their behaviour during analysis is supposed to be the same of the sample (Sylvester, 2008). Thus, each of our bio-apatite in-house standard was analyzed several times (at least 5) during the whole session to observe the external reproducibility on different Sr-concentration materials. Following the method proposed by Horstwood et al. (2008), we built with our bio-standards a calibration

curve based on the accuracy of the $^{87}Sr/^{86}Sr$ ratio (measured value/true value) vs. the inverse of the ^{88}Sr signal ($1/^{88}Sr$). Three of the apatites (the shark tooth, the bovine tooth and the swine tooth) were used to build the daily calibration curve, while the human tooth was used only to check the precision and accuracy of the analysis on low-Sr samples. This daily LA calibration line ($r^2 = 0.82$; $p < 0.00001$; $n = 18$) results in a slope of 0.0005954 and an intercept of 1.0000077 (Fig. 4). We also built a calibration curve ($r^2 = 0.99$) based on the 2σ of the standard materials vs. the inverse of the Sr concentration (1/Sr) to obtain the external reproducibility of an unknown sample with a given Sr concentration. Sr concentrations of our standards have been previously measured by LA–ICP–MS for comparison.

The daily $^{84}Sr/^{86}Sr$ ratio is 0.05609 ± 0.00088 (2σ), which is, within error, equal to the natural 0.0565 ratio (for a detailed review of the significance of this ratio see Horstwood et al., 2008; Vroon et al., 2008).

All LA results of our standard materials are reported in Table 2. The LA analysis of the human tooth (Sr c.a. 100 ppm) yielded an average value of 0.70917 ± 0.00050, which is identical to the true value by dissolution MC–ICP–MS (0.70917 ± 0.00001; 2SE). The swine tooth (Sr c.a. 250 ppm), after the calibration correction, yielded a $^{87}Sr/^{86}Sr$ ratio of 0.70897 ± 0.00012 (2σ), equal to the dissolution result (0.70900 ± 0.00001; 2SE). The bovine tooth standard (Sr c.a. 350 ppm), after correction, yielded a mean $^{87}Sr/^{86}Sr$ ratio of 0.70881 ± 0.00008 (2σ), equal within error to the dissolution value (0.70877 ± 0.00001; 2SE). The shark tooth (Sr c.a. 1100 ppm), yielded a mean corrected $^{87}Sr/^{86}Sr$ ratio of 0.70916 ± 0.00004 (2σ), identical within error to the modern Indian Ocean seawater (~0.70918; Mokadem et al., 2015) and to the ratio obtained by dissolution method (0.70919 ± 0.00001; 2SE).

3. Results

3.1. Retzius line counting

Retzius lines were counted only in sample RH–IS26 because it was the best available tooth fragment with the proper orientation for this type of observations (Fig. 5).

Relying on visible striae, we have estimated the presence of c.a. 30–35 Retzius lines along the entire length of the enamel and of about 10–15 lines along the OES. The number of laminations per Retzius band (i.e. periodicity) is 7, in agreement with the observations of Tafforeau et al. (2007). Thus, sample RH–IS26 should cover a period of about 200–250 days along the EDJ and of about 80–100 days along the OES. In the upper part of the sample (nearest to the apex), we approximately calculated an outward extension rate of the enamel of about 0.5 mm/month (~ 15 µm/d) in agreement with literature data (e.g. Tafforeau et al., 2007; Bendrey et al., 2015).

3.2. Dissolution Sr isotopes

The enamel portions of the two rhinos yielded bulk $^{87}Sr/^{86}Sr$ ratios of 0.70952 ± 0.00001 (2SE, 100 cycles per analysis) and 0.70979 ± 0.00001 (2SE, 100 cycles per analysis), for RH–IS30 and RH–IS26 respectively.

All dissolution results, including those of the standard materials, are reported in Table 2.

3.3. *In situ* LA Sr isotopes

The whole dataset of RH–IS30 and RH–IS26 $^{87}Sr/^{86}Sr$ ratios is reported in Table 3. The mean $^{87}Sr/^{86}Sr$ ratio of all LA analyses of RH–IS30 enamel is 0.70951 ± 0.00014

(2σ, *n* = 42), i.e., identical to the ratio obtained by dissolution (0.70952 ± 0.00001). The $^{87}Sr/^{86}Sr$ ratios, however, vary significantly within the RH–IS30 enamel ranging from 0.70966 to 0.70938. The mean $^{87}Sr/^{86}Sr$ value of LA dentine analyses is 0.70918 ± 0.00013 (2σ, *n* = 10), a ratio quite similar to modern seawater (~0.70917; Dia et al., 1992). Using our standard materials with known Sr concentrations, we have also calculated a Sr concentration of 361 ± 49 ppm (2σ) in the enamel and 447 ± 76 ppm (2σ) in the dentine for sample RH–IS30.

The mean LA $^{87}Sr/^{86}Sr$ value of RH–IS26 enamel is 0.70976 ± 0.00015 (2σ, *n* = 20), identical to the true value by dissolution (0.70979 ± 0.00001). Similarly to sample RH–IS30, we observe a high variability of the $^{87}Sr/^{86}Sr$ ratios within the enamel, with values ranging between 0.70997 and 0.70950. The mean $^{87}Sr/^{86}Sr$ ratio of LA dentine analyses is 0.70934 ± 0.00009 (2σ, *n* = 10), a value more radiogenic than modern seawater (~0.70917). The interpolated Sr concentration for RH–IS26 enamel is 509 ± 131 ppm (2σ) while the dentine is 544 ± 131 ppm (2σ).

3.4. Diagenesis

Both teeth show significant isotopic variability along the enamel surface (Fig. 1 and 2). Enamel, unlike dentine (e.g. Lee-Thorp and Sponheimer, 2003; Bentley, 2006), is rarely affected by diagenetic contamination even in prehistoric samples (Budd et al., 2000), we can, therefore, consider these variations as real. The $^{87}Sr/^{86}Sr$ ratio of dentine, however, is still an important information because is used as the reference value for the “local” substrate isotopic signature (e.g. Bentley, 2006; Britton et al, 2011). This is due to the large pores (1µm tubules) of dentine that make this tissue highly susceptibility to diagenetic alteration (Kohn et al., 1999) especially in prehistoric samples. Any significant Sr enrichment in dentine can be due to the effect

of local diagenetic contamination and/or animal physiology (see Evans et al., 2006). Sample RH–IS30 shows a dentine-enamel difference of 86 ppm, while sample RH–IS26 of 35 ppm. The smaller Sr concentration difference of sample RH–IS26 might be interpreted as a minor diagenetic alteration for this sample that in fact retains a $^{87}Sr/^{86}Sr$ ratio (0.70934) higher than sample RH–IS30 (0.70918) and perhaps less affected by the modern seawater signal of 0.7092, that locally dominates the Sr rainwater isotopic composition (e.g. Montgomery, 2010). Therefore, we can infer that the local Sr isotope signature should be lower than ~0.7093, probably close to modern seawater.

3.5. External reproducibility

The external reproducibility is the error associated with repeated measurements of reference standard materials, generally expressed as a multiple of the standard deviation.

We calculated an external reproducibility of 0.00008 (2σ) for sample RH–IS30, whereas the interpolated external reproducibility is 0.00005 (2σ) for sample RH–IS26 (see section 2.3 of this paper for more details). Therefore, we consider all values outside this range as significantly different Sr isotopic compositions that can be related to morphological growth features of the teeth as discussed in the following section.

4. Discussion

4.1. Rhino tooth growth and Sr isotopic composition

The estimated crown formation time of rhino species ranges between about 1.5 and 3

years (Tafforeau et al., 2007; Hillman-Smith et al., 1986), a long enough period during which the animal may have migrated through the landscape. For all the profiles we studied at the microscope and analysed by LA, we approximately followed the growth direction of the enamel (e.g. Tafforeau et al., 2007; Bentley, 2006; Khon et al., 2002), trying to observe possible seasonal variations both in the growth features and in the Sr isotopic composition. Because dentine growth direction is inward from the EDJ, those portions of the profiles that include dentine samples are inverted in terms of tissue growth. However, because of the observed diagenetic contamination of dentine, we considered this tissue as a homogeneous matrix, ignoring any possible incremental feature.

4.1.1. Tooth sample RH–IS30

The RH–IS30 sample is a horizontal section of a rhino molar fragment, but given that enamel nucleates at EDJ and grows downward from the tooth crown and outward from the EDJ itself, it is difficult to determine the precise time-span that this tooth section covers. In large herbivores, namely horses from Kohn et al. (2002), the outward growth rate is about 1 mm/month (Kohn et al., 2002). Given that the enamel thickness of RH–IS30 sample is about 2 mm, the time recorded by this sample should be at least 2 months, or even longer considering that rhino enamel growth seems slightly slower than the one of a horse (Bendrey et al., 2015; Tafforeau et al., 2007; Kohn et al., 2002). RH–IS26 sample, based on the observation of laminations, revealed an outward growth rate of about 0.5 mm/month in agreement with the growth rate of rhino teeth (Tafforeau et al. 2007). This suggests a recorded time span of about 3-4 months for sample RH–IS30. Both Sr isotope profiles obtained for this sample follow the outward direction (from the EDJ) of the enamel growth. Profile A,

composed by 32 small linear analyses, covers the entire length of the sample with the first line near the EDJ and the last line close to the external surface (Fig. 1). This profile includes relatively regular cyclic variations of the $^{87}Sr/^{86}Sr$ ratio, from highly radiogenic ratios (>0.70960) to less radiogenic ratios (<0.70945). A simple t-test (>0.70960, single sample one-tailed t-test p = 0.02; <0.70945, p = 0.04) shows that these ratios are statistically different from the mean of the profile (0.70953). Profile B, measured half within the enamel and half within the dentine, also shows cyclic variations of the Sr isotopic ratios but with higher periodicity and clearly displays the chemical boundary between the enamel and the dentine. The enamel part of the profile includes only one value (0.70957) statistically different from the mean value of the profile itself.

4.1.2. Tooth sample RH–IS26

Sample RH–IS26 is a vertical section of a rhino molar fragment. For this sample, we analyzed both the exposed inner surface (Fig. 2) and the external surface (OES, Fig. 3) of the enamel. We observe cyclic variations of the Sr isotopic composition in both profiles with different periodicity. Theoretically, the OES and the exposed internal surface should encrypt similar incremental information. However, Tafforeau et al. (2007) showed how the external and the internal surface (along the EDJ) of the rhino enamel have different growth rate. When Retzius lines reach the OES of the enamel, they form ridges called perikymata (e.g. Smith and Tafforeau, 2008). Our sample represents the last ~ 8 mm (distance from the cervix) of the crown. Hence, the internal exposed surface of the enamel based on rates by Tafforeau et al. (2007) should represents a time-span of about 300–350 days, while the external surface a time-span of about 100 days. Our counting of Retzius lines agrees well with these

estimates, revealing at least a time-interval of about 200–250 days along the EDJ and of 80 days along the OES.

According to the different growth rate between OES and inner surface, we observe that the second half of the Sr isotopic composition profile E seems to reflect the same fluctuations of the entire length of the F profile. In Figure 3c we compared the two profiles and shifted them to obtain the strongest possible correlation (r^2 = 0.56; p < 0.00001), confirming the fact that the two profiles show equivalent temporal variations in Sr isotopic composition. In addition, the other two profiles (C and D), which should encrypt fewer (about 2) months of the rhino life, display similar cyclical variations.

4.2. Rhino seasonal movements

Given that the Sr isotopic composition of the growing rhinos teeth derives from the land where the animal lived, these cyclic variations of the $^{87}Sr/^{86}Sr$ ratio likely indicate different water and food intake and, therefore, seasonal movements of the two animals to different lands, e.g. with different Sr isotopic composition. Even the shorter time range (about 100 days) observed seems to be characterized by cyclic variations of the $^{87}Sr/^{86}Sr$ ratio and consequently of the migration pattern. Moreover, both tooth samples show an enamel $^{87}Sr/^{86}Sr$ ratio considerably higher than its relative dentine ratio that represents the local water/food signal (0.70951 vs. 0.70918 for RHIS–30, one-tailed Mann-Whitney U-test p = 0.04; 0.70976 vs. 0.70934 for RH–IS26, one-tailed Mann-Whitney U-test p = 0.06).

We try now to identify the Sr reservoir responsible for the chemical variations observed in the rhinos. The site of Isernia and the surrounding area are characterized by Holocene and Pleistocene fluvial deposits and limestone and dolostone ranging between the Cretaceous and the Holocene (Peretto et al., 2015). Therefore, the

$^{87}Sr/^{86}Sr$ isotopic composition of these rocks should range approximately between 0.7073 and 0.7092 according to the global Sr isotopes seawater curve of McArthur et al. (2001). This is a big interval, however, our samples have even higher $^{87}Sr/^{86}Sr$ ratios. One of the possible sources of the more radiogenic ratios of our samples can be identified in the Roccamonfina volcano, located 50 km to the southeast of Isernia. Previous geological work has shown that the lavas from the 630 ka eruption of the Roccamonfina volcano have a $^{87}Sr/^{86}Sr$ isotopic signature ranging between about 0.7093 and 0.7100 (Conticelli et al., 2009). In addition, located about 150 km to the northeast of Isernia, the Middle-Pleistocene Colli Albani volcano lavas show $^{87}Sr/^{86}Sr$ ratios higher than 0.7100 (Giaccio et al., 2013; Boari et al., 2009). Likely, our Isernia Rhinos have travelled to these volcanic grounds and fed themselves with water/food "contaminated" with highly radiogenic $^{87}Sr/^{86}Sr$ ratios.

According to palaeoenvironmental reconstructions, the Isernia La Pineta environment consisted of an association of closed forests, grasslands and semi-open woodlands (Orain et al., 2013; Thun Hohenstein et al., 2004), seemingly a good ground for rhinos grazing. However, based on our data, these rhinos were very mobile and seasonally reached the fertile substratum offered by the volcanic soils (Ugolini and Zasoski, 1979). Understanding the specific direction of the rhinos movements (either to the Roccamonfina volcano or to the Colli Albani area) remains no more than a speculation. Yet, we can certainly state that the Isernia rhinos have seasonally migrated as shown by the Sr isotopic composition temporal variations measured in their teeth, covering a distance of at least 50 km and returned cyclically to Isernia La Pineta or to a different site, but farther away from the isotopic influence of the volcanos.

Conclusions

We exploited the LA–MC–ICP–MS technique to study ancient animal migration patterns of two *Stephanorhinus hundsheimensis* teeth discovered in the Middle Pleistocene site of Isernia La Pineta, where the most ancient human Italian tooth has been unearthed. The two teeth, here analysed in high-spatial resolution, revealed time-related fluctuations of the Sr isotopic composition, likely linked to seasonal movements of the rhinos, probably towards the more fertile volcanic soils of Roccamonfina and/or Colli Albani. Moreover, while dentine has been possibly altered by diagenetic processes, enamel seems to be pristine and therefore suitable for reliable Sr isotopic analysis. As expected, both the inner and the outer enamel surface of the vertically sectioned sample, RH–IS26, showed highly correlated variations of the $^{87}Sr/^{86}Sr$ ratio, but with different time spans, related to the differential growth rate of the tooth portions. Additionally, we have successfully investigated the $^{87}Sr/^{86}Sr$ ratio of low-Sr (to c.a. 100 ppm) bioapatites, using three matrix-matched standards to correct unresolved interferences arising from LA analyses.

Acknowledgments

This work was supported by the “Programma Giovani Ricercatori Rita Levi Montalcini” to AC. We are grateful to Matteo Reghizzi, Marie Catherine Sforna, Daniela Manzini and Maria Cecilia Rossi for their precious help during the analytical sessions. We would also like to thank Stefano Benazzi for his constant support and encouragement, Aurora Pederzoli for donating the archaeological swine and bovine samples and two anonymous reviewers for their comments and suggestions. We are

also indebted to Paul Tafforeau for his helpful advices with tooth histology.

References

Balasse, M., 2003. Potential biases in sampling design and interpretation of intra-tooth isotope analysis. Int. J. Osteoarchaeol. 13, 3–10. doi:10.1002/oa.656

Ballatore, M., Breda, M., 2013. Stephanorhinus hundsheimensis (Rhinocerontidae, Mammalia) teeth from the early Middle Pleistocene of Isernia La Pineta (Molise, Italy) and comparison with coeval British material. Quat. Int. 302, 169–183. doi:10.1016/j.quaint.2013.02.002

Balter, V., Braga, J., Télouk, P., Thackeray, J.F., 2012. Evidence for dietary change but not landscape use in South African early hominins. Nature 489, 558–560. doi:10.1038/nature11349

Balter, V., Telouk, P., Reynard, B., Braga, J., Thackeray, F., Albarède, F., 2008. Analysis of coupled Sr/Ca and 87Sr/86Sr variations in enamel using laser-ablation tandem quadrupole-multicollector ICPMS. Geochim. Cosmochim. Acta 72, 3980–3990. doi:10.1016/j.gca.2008.05.048

Bendrey, R., Vella, D., Zazzo, A., Balasse, M., Lepetz, S., 2015. Exponentially decreasing tooth growth rate in horse teeth: Implications for isotopic analyses. Archaeometry 57, 1104–1124. doi:10.1111/arcm.12151

Bentley, R.A., Bickle, P., Fibiger, L., Nowell, G.M., Dale, C.W., Hedges, R.E.M., Hamilton, J., Wahl, J., Francken, M., Grupe, G., Lenneis, E., Teschler-Nicola, M., 2012. Community differentiation and kinship among Europe's first farmers. PNAS 109, 9326–9330. doi:10.1073/pnas.1113710109

Bentley, R.A., 2006. Strontium isotopes from the earth to the archaeological skeleton: A review. J. Archaeol. Method Theory 13, 135–187. doi:10.1007/s10816-006-9009-x

Boari, E., Avanzinelli, R., Melluso, L., Giordano, G., Mattei, M., Benedetti, A.A. De, Morra, V., Conticelli, S., 2009. Isotope geochemistry (Sr–Nd–Pb) and petrogenesis of leucite-bearing volcanic rocks from "Colli Albani" volcano, Roman Magmatic Province, Central Italy: inferences on volcano evolution and magma genesis 977–1005. doi:10.1007/s00445-009-0278-6

Britton, K., Grimes, V., Niven, L., Steele, T.E., McPherron, S., Soressi, M., Kelly, T.E., Jaubert, J., Hublin, J.J., Richards, M.P., 2011. Strontium isotope evidence for migration in late Pleistocene Rangifer: Implications for Neanderthal hunting strategies at the Middle Palaeolithic site of Jonzac, France. J. Hum. Evol. 61, 176–185. doi:10.1016/j.jhevol.2011.03.004

Budd, P., Montgomery, J., Barreiro, B., Thomas, R.G., 2000. Differential diagenesis of strontium in archaeological human dental tissues. Appl. Geochemistry 15, 687–694. doi:10.1016/S0883-2927(99)00069-4

Burton, J.H., Price, D.T., Middleton, W.D., 1999. Correlation of Bone Ba/Ca and Sr/Ca due to Biological Purification of Calcium. J. Archaeol. Sci. 26, 609–616.

Burton, J.H., Wright, L.E., 1995. Nonlinearity in the Relationship Between Bone Sr/Ca and Diet: Paleodietary Implications. Am. J. Phys. Anthropol. 96, 273–282.

Coltorti, M., Feraud, G., Marzoli, A., Peretto, C., Ton-That, T., Voinchet, P., Bahain, J.J., Minelli, A., Thun Hohenstein, U., 2005. New 40Ar/39Ar, stratigraphic and palaeoclimatic data on the Isernia La Pineta Lower Palaeolithic site, Molise, Italy. Quat. Int. 131, 11–22. doi:10.1016/j.quaint.2004.07.004

Conticelli, S., Marchionni, S., Rosa, D., Giordano, G., Boari, E., Avanzinelli, R., 2009. Shoshonite and sub-alkaline magmas from an ultrapotassic volcano: Sr-Nd-Pb isotope data on the Roccamonfina volcanic rocks, Roman Magmatic Province, Southern Italy. Contrib. to Mineral. Petrol. 157, 41–63. doi:10.1007/s00410-008-0319-8

Copeland, S.R., Sponheimer, M., le Roux, P.J., Grimes, V., Lee-Thorp, J.A., de Ruiter, D.J., Richards, M.P., 2008. Strontium isotope ratios ($^{87}Sr/^{86}Sr$) of tooth enamel: a comparison of solution and laser ablation multicollector inductively coupled plasma mass spectrometry methods. Rapid Commun. Mass Spectrom. 22, 3187–3194. doi:10.1002/rcm

Copeland, S.R., Sponheimer, M., Lee-Thorp, J.A., le Roux, P.J., de Ruiter, D.J., Richards, M.P., 2010. Strontium isotope ratios in fossil teeth from South Africa: assessing laser ablation MC-ICP-MS analysis and the extent of diagenesis. J. Archaeol. Sci. 37, 1437–1446. doi:10.1016/j.jas.2010.01.003

Copeland, S.R., Sponheimer, M., de Ruiter, D.J., Lee-Thorp, J.A, Codron, D., le Roux, P.J., Grimes, V., Richards, M.P., 2011. Strontium isotope evidence for landscape use by early hominins. Nature 474. doi:10.1038/nature

Davidson, J., Tepley, F., Palacz, Z., Meffan-Main, S., 2001. Magma recharge, contamination and residence times revealed by in situ laser ablation isotopic analysis of feldspar in volcanic rocks. Earth Planet. Sci. Lett. 184, 427–442. doi:10.1016/S0012-821X(00)00333-2

Deniel, C., Pin, C., 2001. Single-stage method for the simultaneous isolation of lead and strontium from silicate samples for isotopic measurements. Anal. Chim. Acta 426(1), 95–103.

Dia, A., Cohen, A., O'Nions, R., Shackleton, N., 1992. Seawater Sr isotope variation over the past 300 kyr and influence of global climate cycles. Nature 356.

Durante, C., Baschieri, C., Bertacchini, L., Bertelli, D., Cocchi, M., Marchetti, A., Manzini, D., Papotti, G., Sighinolfi, S., 2015. An analytical approach to Sr isotope ratio determination in Lambrusco wines for geographical traceability purposes. Food Chem. 173, 557–563. doi:10.1016/j.foodchem.2014.10.086

Enax, J., Prymak, O., Raabe, D., Epple, M., 2012. Structure, composition, and mechanical properties of shark teeth. J. Struct. Biol. 178, 290–299. doi:10.1016/j.jsb.2012.03.012

Evans, J.A., Chenery, C.A., Fitzpatrick, A.P., 2006. Bronze Age childhood migration of individuals near Stonehenge, revealed by strontium and oxygen isotope tooth enamel analysis. Archaeometry 48, 309–321.

Giaccio, B., Arienzo, I., Sottili, G., Castorina, F., Gaeta, M., Nomade, S., Galli, P., Messina, P., 2013. Isotopic (Sr e Nd) and major element fingerprinting of distal tephras: an application to the Middle-Late Pleistocene markers from the Colli Albani volcano, central Italy. Quat. Sci. Rev. 67, 190–206. doi:10.1016/j.quascirev.2013.01.028

Guillong, M., Günther, D., 2002. Effect of particle size distribution on ICP-induced elemental fractionation in laser ablation-inductively coupled plasma-mass spectrometry. J. Anal. At. Spectrom. 17, 831–837. doi:10.1039/b202988j

Hillman-Smith, A.K.K., Owen-Smith, N., Anderson, J.L., Hall- Martin, A.J., Selaladi, J.P., 1986. Age estimation of the white rhinoceros (Ceratotherium simum). J. Zool. 210, 355–379.

Horn, I., 2008. Comparison of femtosecond and nanosecond laser interactions with geologic matrices and their influence on accuracy and precision of LA–ICP–MS data. In: Sylvester, P.J. (Ed.), Laser Ablation ICP-MS in the Earth Sciences: Current Practices and Outstanding Issues. Mineralogical Association of Canada, pp. 53–66.

Horstwood, M.S.A., Nowell, G.M., 2005. Multi–collector devices. In: Nelms S. (Ed.), Inductively Coupled Plasma Mass Spectrometry Handbook. Blackwell Scientific Publications, pp. 54–68.

Horstwood, M.S.A., Evans, J.A., Montgomery, J., 2008. Determination of Sr isotopes in calcium phosphates using laser ablation inductively coupled plasma mass spectrometry and their application to archaeological tooth enamel. Geochim. Cosmochim. Acta 72, 5659–5674. doi:10.1016/j.gca.2008.08.016

Jackson, M.G., Hart, S.R., 2006. Strontium isotopes in melt inclusions from Samoan basalts: Implications for heterogeneity in the Samoan plume. Earth Planet. Sci. Lett. 245, 260–277. doi:10.1016/j.epsl.2006.02.040

Kohn, M.J., Miselis, J.L., Fremd, T.J., 2002. Oxygen isotope evidence for preogressive uplift of the Cascade Range, Oregon. Earth Planet. Sci. Lett. 204, 151–165. doi:10.1016/S0012-821X(02)00961-5

Kohn, M.J., Schoeninger, M.J., Barker, W.W., 1999. Altered states: effects of diagenesis on fossil tooth chemistry. Geochim. Cosmochim. Acta 18, 2737-2747.

Lee-Thorp, J., Sponheimer, M., 2003. Three case studies used to reassess the reliability of fossil bone and enamel isotope signals for paleodietary studies. J. Anthropol. Archaeol. 22, 208–216. doi:10.1016/S0278-4165(03)00035-7

Lewis, J., Coath, C.D., Pike, A.W.G., 2014. An improved protocol for $^{87}Sr/^{86}Sr$ by laser ablation multi-collector inductively coupled plasma mass spectrometry using oxide reduction and a customised plasma interface. Chem. Geol. 390, 173–181. doi:10.1016/j.chemgeo.2014.10.021

Li, Z., He, M., Peng, B., Jin, Z., 2013. Strontium concentrations and isotope ratios in enamel of healthy and carious teeth in southern Shaanxi, China. Rapid Commun. Mass Spectrom. 27, 1919–1924. doi:10.1002/rcm.6646

Lugli, F., Brunelli, D., Cipriani, A., Bosi, G., Traversari, M., Gruppioni, G., *accepted*. C_4-plant foraging in Northern Italy: stable isotopes, Sr/Ca and Ba/Ca data of human osteological samples from Roccapelago (16^{th}–18^{th} century AD). Archaeometry.

Martin, C., Bentaleb, I., Kaandorp, R., Iacumin, P., Chatri, K., 2008. Intra-tooth study of modern rhinoceros enamel δ18O: Is the difference between phosphate and carbonate δ18O a sound diagenetic test? Palaeogeogr. Palaeoclimatol. Palaeoecol. 266, 183–189. doi:10.1016/j.palaeo.2008.03.039

McArthur, J.M., Howarth, R.J., Bailey, T.R., 2001. Strontium isotope stratigraphy: LOWESS version 3: best fit to the marine Sr-isotope curve for 0-509 Ma and accompanying look-up table for deriving numerical age. J. Geol. 109 (2), 155–170.

Mokadem, F., Parkinson, I.J., Hathorne, E.C., Anand, P., Allen, J.T., Burton, K.W., 2015. High-precision radiogenic strontium isotope measurements of the modern and glacial ocean : Limits on glacial – interglacial variations in continental weathering. Earth Planet. Sci. Lett. 415, 111–120. doi:10.1016/j.epsl.2015.01.036

Montgomery, J., 2010. Passports from the past: Investigating human dispersals using strontium isotope analysis of tooth enamel. Ann. Hum. Biol. 37, 325–346. doi:10.3109/03014461003649297

Montgomery, J., Evans, J.A., Cooper, R.E., 2007. Resolving archaeological populations with Sr-isotope mixing models. Appl. Geochemistry 22, 1502–1514. doi:10.1016/j.apgeochem.2007.02.009

Müller, W., Anczkiewicz, R., 2016. Accuracy of Laser-Ablation (LA)-MC-ICPMS Sr Isotope Analysis of (Bio)Apatite – a Problem Reassessed. J. Anal. At. Spectrom. 31, 259–269. doi:10.1039/C5JA00311C

Nowell, G.M., Horstwood, M.S.A., 2009. Comments on Richards et al., Journal of Archaeological Science 35, 2008 “Strontium isotope evidence of Neanderthal mobility at the site of Lakonis, Greece using laser-ablation PIMMS.” J. Archaeol. Sci. 36, 1334–1341. doi:10.1016/j.jas.2009.01.019

Orain, R., Lebreton, V., Russo Ermolli, E., Sémah, A.M., Nomade, S., Shao, Q., Bahain, J.J., Thun Hohenstein, U., Peretto, C., 2013. Hominin responses to environmental changes during the Middle Pleistocene in central and southern Italy. Clim. Past 9, 687–697. doi:10.5194/cp-9-687-2013

Pate, F.D., 1994. Bone chemistry and paleodiet. J. Archaeol. Method Theory 1, 161–209. doi:10.1007/BF02231415

Peretto, C., Arnaud, J., Moggi-Cecchi, J., Manzi, G., Nomade, S., Pereira, A., et al., 2015. A human deciduous tooth and new 40Ar/39Ar dating results from the Middle Pleistocene archaeological site of Isernia La pineta, southern Italy. PLoS One 10, 1–19. doi:10.1371/journal.pone.0140091

Price, D.T., Burton, J.H., Bentley, R.A., 2002. The Characterization Of Biologically Available Strontium Isotope Ratios For The Study Of Prehistoric Migration. Archaeometry 44, 117–135.

Richards, M., Harvati, K., Grimes, V., Smith, C., Smith, T., Hublin, J.-J., Karkanas, P., Panagopoulou, E., 2008. Strontium isotope evidence of Neanderthal mobility at the site of Lakonis, Greece using laser-ablation PIMMS. J. Archaeol. Sci. 35, 1251–1256. doi:10.1016/j.jas.2007.08.018

Simonetti, A., Buzon, M.R., Creaser, R.A., 2008. In-Situ Elemental And Sr Isotope Investigation Of Human Tooth Enamel By Laser Ablation-(MC)-ICP-MS: Successes And Pitfalls. Archaeometry 50, 371–385. doi:10.1111/j.1475-4754.2007.00351.x

Smith, T.M., Tafforeau, P., 2008. New visions of dental tissue research: Tooth development, chemistry, and structure. Evol. Anthropol. 17, 213–226. doi:10.1002/evan.20176

Sylvester, P.J., 2008. Matrix Effects in Laser Ablation-ICP-MS. In: Sylvester, P.J. (Ed.), Laser Ablation ICP-MS in the Earth Sciences: Current Practices and Outstanding Issues. Mineralogical Association of Canada, pp. 67–78.

Tafforeau, P., Bentaleb, I., Jaeger, J.J., Martin, C., 2007. Nature of laminations and mineralization in rhinoceros enamel using histology and X-ray synchrotron

microtomography: Potential implications for palaeoenvironmental isotopic studies. Palaeogeogr. Palaeoclimatol. Palaeoecol. 246, 206–227. doi:10.1016/j.palaeo.2006.10.001

Thun Hohenstein, U., Malerba, G., Giacobini, G., and Peretto, C., 2004. Bone surface micromorphological study of the faunal remains from the Lower Palaeolithic site of Isernia La Pineta (Molise, Italy), BAR Int. Ser. 1272, Actes du XIV Congrès de l'Union Internationale des Sciences Préhistoriques et Protohistoriques, Oxford, 123–127.

Ugolini, F.C., Zasoski, R.J., 1979. Soils derived from Thephra. In: Sheets, P.D., Grayson, D.K. (Ed.), Volcanic Activity and Human Ecology. Academic Press, pp. 83–124.

Vennemann, T., Hegner, E., Cliff, G., Benz, G., 2001. Isotopic composition of recent shark teeth as a proxy for environmental conditions. Geochim. Cosmochim. Acta 65, 1583–1599.

Vroon, P.Z., van der Wagt, B., Koornneef, J.M., Davies, G.R., 2008. Problems in obtaining precise and accurate Sr isotope analysis from geological materials using laser ablation MC-ICPMS. Anal. Bioanal. Chem. 390, 465–76. doi:10.1007/s00216-007-1742-9

Willmes, M., Kinsley, L., Moncel, M.H., Armstrong, R.A., Aubert, M., Eggins, S., Grün, R., 2016. Improvement of laser ablation in situ micro-analysis to identify diagenetic alteration and measure strontium isotope ratios in fossil human teeth. J. Archaeol. Sci. 70, 102–116. doi:10.1016/j.jas.2016.04.017

Woodhead, J., Swearer, S., Hergt, J., Maas, R., 2005. In situ Sr-isotope analysis of carbonates by LA-MC-ICP-MS: interference corrections, high spatial resolution and an example from otolith studies. J. Anal. At. Spectrom. 20, 22–27. doi:10.1039/b412730g

Fig. 1. a. RH–IS30 sample photo, with visible Hunter-Schreger bands. **b.** Profile A is composed by 32 small (100 x 500 µm) LA analyses; blue line is the average of the analyses; grey area is the 2σ-error of 0.00008 calculated from the standard materials; x-error bars are the 2-standard errors. **c.** Profile B starts from the dentine and proceeds outward to the OES; while for enamel the profile follows the tooth growth, for dentine the direction is inverted (see text for details); symbols are the same as in profile A. **d.** Example of a tooth horizontal section (redrawn from Ballatore and Breda, 2013).

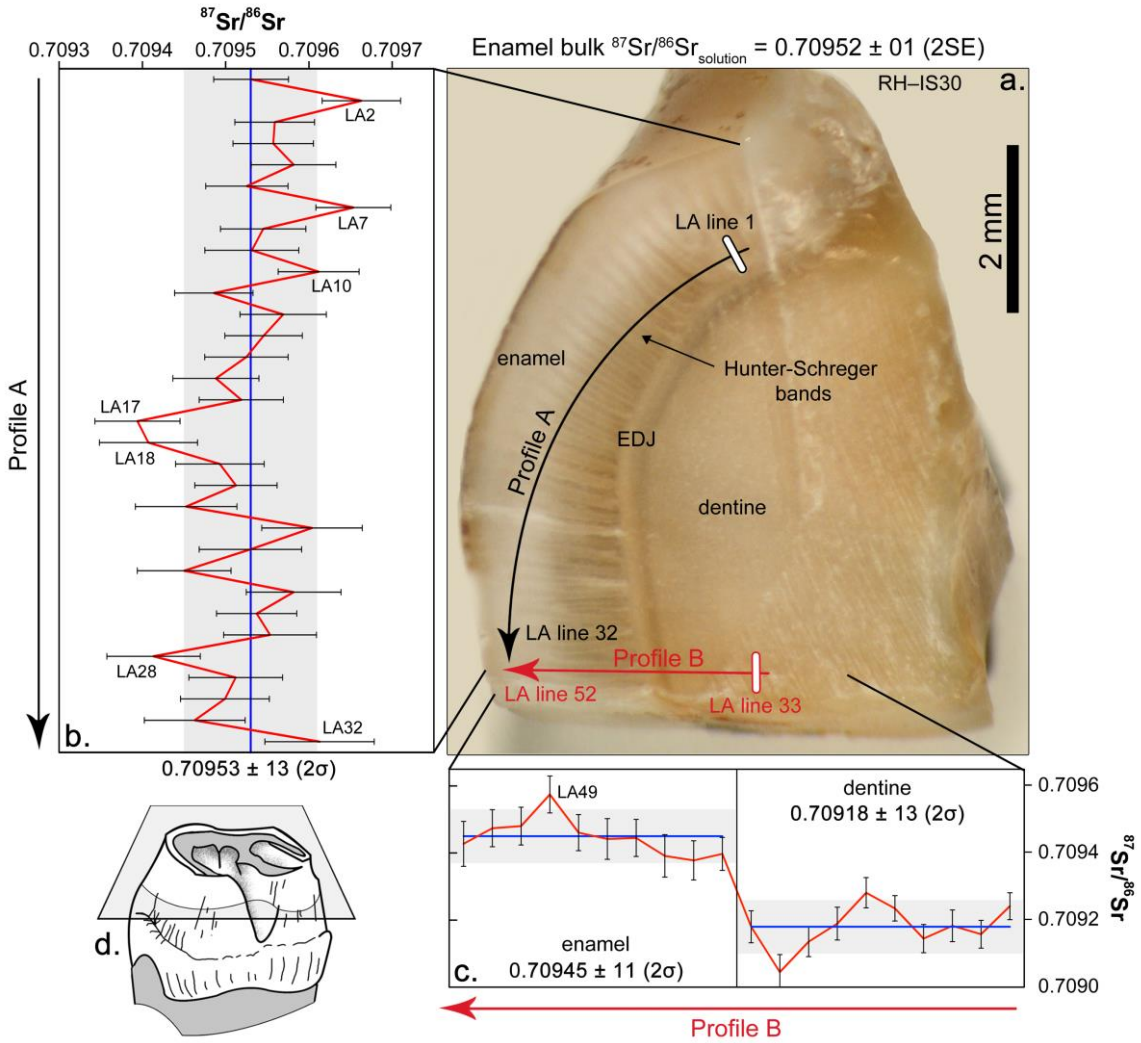

Fig. 2. a. RH–IS26 sample photo of the exposed inner surface. **b.** Profile C cover a short portion of the enamel near the OES and is composed by 11 LA analyses; blue line is the average of the analyses; grey area is the 2σ-error of 0.00005 calculated from the standard materials; x-error bars are the 2-standard errors. **c.** Profile D starts from the dentine and proceeds outward to the OES; while for enamel the profile follows the tooth growth, for dentine the direction is inverted (see text for details); symbols are the same as in profile C. **d.** Profile E is a single LA analysis which cover all the length of the enamel, reported as a moving average with a period of 100; symbols are the same as in profile D. **e.** Example of a tooth vertical section (redrawn from Ballatore and Breda, 2013).

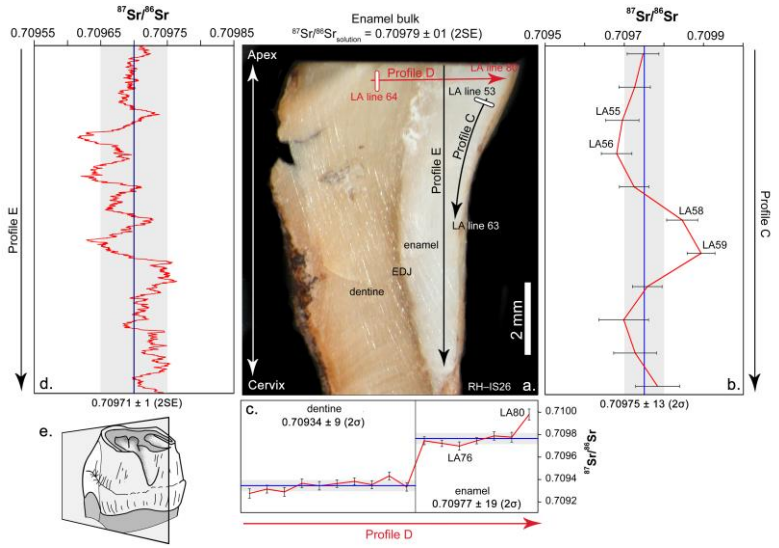

Fig. 3. a. RH–IS26 sample photo of the outer enamel surface (OES). **b.** Profile F is a single LA analysis which cover all the length of the outer enamel, reported as a moving average with a period of 100; blue line is the average of the analyses; grey area is the 2σ-error of 0.00005 calculated from the standard materials. **c.** Comparison between profile F and the second half of profile E (Fig. 2d); the two profiles show a high correlation ($r^2 = 0.56$). For a better visual comparison, profile E, which has relatively less data, is smoothed with a Savitzky–Golay filter.

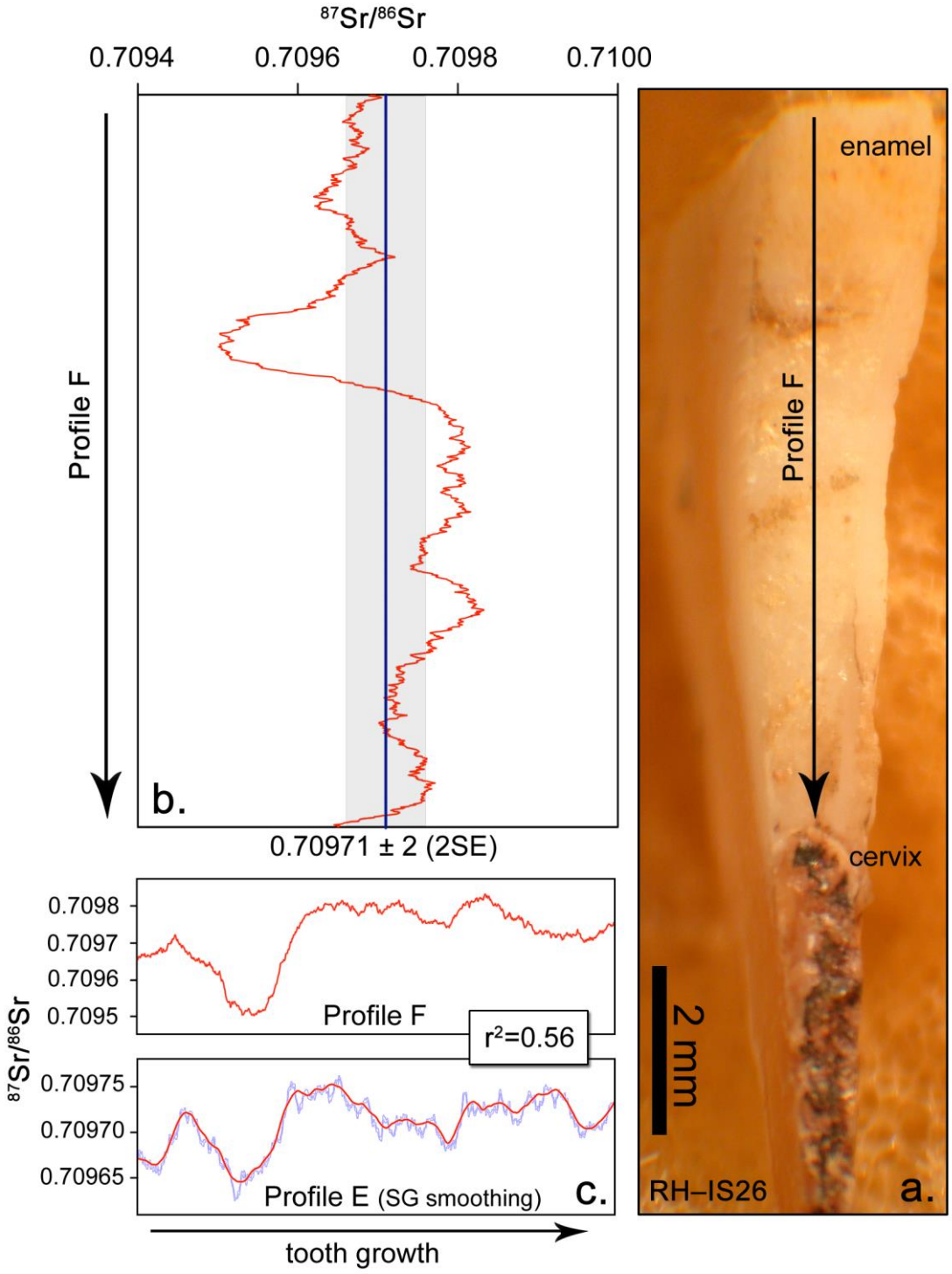

Fig. 4. Correlation between the accuracy of the $^{87}Sr/^{86}Sr$ analysis (observed/true) and the inverse of the ^{88}Sr signal. This high correlation is attributed by some authors to the Ca–P–O interference which occurs during LA analysis of bioapatites (see text for details). The line equation is used to correct our LA data.

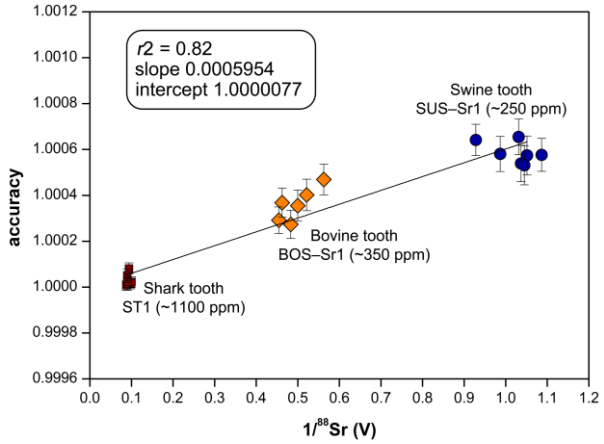

Fig. 5. Retzius line observation under polarized transmitted light with a petrographic microscope on RH–IS26

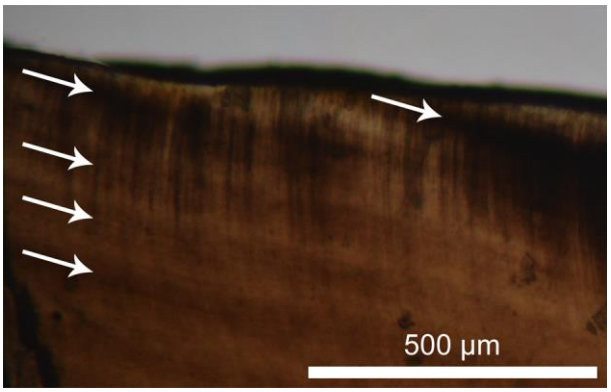

Table 1. Parameters and operating conditions for Sr isotope determination by laser ablation MC–ICP–MS

Parameters	**Values**
Laser ablation New Wave Up 213	
Wavelength	213 nm
He flow rate	0.6 L/min
Ablation	
Spot size	100 µm
Frequency	10 Hz
Fluence	~20 J/cm^2
Sampling scheme	Line (dynamic)
Line translation rate	5 µms^{-1}
Pre–ablation	
Spot size	100 µm
Frequency	10 Hz
Line translation rate	40 µms^{-1}
MC–ICP–MS Neptune	
Cool gas flow rate	15 L/min
Auxiliary gas flow	0.8 L/min
Sample gas flow	0.9 – 1 L/min
Plasma power	1200
Resolution	Low (450)
Collected masses	^{88}Sr (H4), ^{87}Sr (H3), 86.5 (H2), ^{86}Sr (H1), 85.5 (C), ^{85}Rb (L1), ^{84}Sr, (L2) ^{83}Kr (L3), ^{82}Kr (L4)
Data collection	1 block, 200 cycles, 0.5 s integration

Table 2
MC-ICP–MS $^{87}Sr/^{86}Sr$ data and Sr concentrations of the bioapatites used as standard materials.

Sample	Solution $^{87}Sr/^{86}Sr$ (±2SE)	LA corrected $^{87}Sr/^{86}Sr$ (±2σ)	Sr concentration (ppm)	Characteristics	Provenance
ST1 – A	0.70918 ± 0.00001	0.70916 ± 0.00004	1101 ± 47	Modern shark tooth	Indian Ocean
ST1 – B	0.70919 ± 0.00001	–	–	–	–
ST1 – C	0.70918 ± 0.00001	–	–	–	–
BOS–Sr1	0.70877 ± 0.00001	0.70881 ± 0.00008	347 ± 18	Archaeological cattle tooth	P.zza Anita Garibaldi Roman site, Ravenna
SUS–Sr1	0.70899 ± 0.00001	0.70897 ± 0.00012	253 ± 31	Archaeological swine tooth	P.zza Anita Garibaldi Roman site, Ravenna
ROCht421*	0.70917 ± 0.00001	0.70917 ± 0.00050	104 ± 25	Archaeological human tooth	Roccapelago post-medieval site, Modena

Letters after the sample name indicate duplicate analyses of a different portion of the same tooth.
*This sample was used only to check the accuracy of the correction. It was not used to build the daily calibration line.

Table 3
$^{87}Sr/^{86}Sr$ results for samples RH–IS30 and RH–IS26. Each analysis represents a short linear scan except for profiles E and F that are long continuous scans

Tooth sample	Solution $^{87}Sr/^{86}Sr$ (± 2SE)	LA sample ID	Sr (ppm)	LA corrected $^{87}Sr/^{86}Sr$	2SE
RH–IS30	0.70951 ± 0.00001				
		1	412	0.70953	0.00004
		2	398	0.70966	0.00005
		3	386	0.70956	0.00005
		4	385	0.70956	0.00005
		5	393	0.70958	0.00005
		6	391	0.70953	0.00005
		7	384	0.70965	0.00004
		8	394	0.70955	0.00005
		9	406	0.70953	0.00006
		10	404	0.70961	0.00005
		11	402	0.70949	0.00005
		12	373	0.70957	0.00005
		13	370	0.70955	0.00005
		14	376	0.70952	0.00005
		15	377	0.70949	0.00005
		16	362	0.70952	0.00005
		17	365	0.70939	0.00005
		18	360	0.70941	0.00006
		19	356	0.70949	0.00005
		20	361	0.70951	0.00005
		21	337	0.70945	0.00006
		22	345	0.70960	0.00006
		23	341	0.70953	0.00006
		24	335	0.70945	0.00006
		25	338	0.70958	0.00006
		26	353	0.70954	0.00005
		27	339	0.70955	0.00006
		28	346	0.70941	0.00006
		29	344	0.70951	0.00006
		30	338	0.70950	0.00005
		31	342	0.70946	0.00006
		32	340	0.70961	0.00007
		33*	494	0.70924	0.00004
		34*	484	0.70916	0.00004
		35*	460	0.70918	0.00005
		36*	454	0.70914	0.00004
		37*	498	0.70923	0.00004
		38*	428	0.70928	0.00005
		39*	443	0.70919	0.00005
		40*	414	0.70914	0.00004

		41*	388	0.70905	0.00005
		42*	408	0.70918	0.00005
		43	375	0.70940	0.00005
		44	337	0.70938	0.00006
		45	335	0.70939	0.00006
		46	338	0.70944	0.00006
		47	346	0.70944	0.00006
		48	338	0.70946	0.00005
		49	340	0.70957	0.00006
		50	338	0.70948	0.00006
		51	340	0.70947	0.00006
		52	341	0.70943	0.00007
RH–IS26	0.70979 ± 0.00001				
		53	504	0.70975	0.00004
		54	486	0.70973	0.00004
		55	488	0.70969	0.00004
		56	482	0.70968	0.00004
		57	519	0.70972	0.00004
		58	505	0.70985	0.00004
		59	515	0.70989	0.00004
		60	559	0.70976	0.00004
		61	467	0.70970	0.00006
		62	464	0.70973	0.00005
		63	454	0.70978	0.00006
		64*	555	0.70933	0.00004
		65*	579	0.70943	0.00003
		66*	635	0.70935	0.00004
		67*	620	0.70938	0.00003
		68*	580	0.70936	0.00003
		69*	530	0.70934	0.00004
		70*	506	0.70936	0.00004
		71*	483	0.70928	0.00004
		72*	536	0.70931	0.00003
		73*	415	0.70927	0.00004
		74	415	0.70997	0.00005
		75	460	0.70977	0.00004
		76	545	0.70978	0.00004
		77	655	0.70974	0.00003
		78	573	0.70969	0.00004
		79	645	0.70972	0.00003
		80	570	0.70974	0.00004
		Profile E	437	0.70971	0.00001
		Profile F	438	0.70971	0.00002

* Dentine samples otherwise enamel.